Oligo(aryleneethynylene)s with Terminal Pyridyl Groups: Synthesis and Length Dependence of the Tunneling to Hopping Transition of Single-molecule Conductances

Xiaotao Zhao,[1,⊥] Cancan Huang,[2,⊥] Murat Gulcur,[1] Andrei S. Batsanov,[1] Masoud Baghernejad,[2] Wenjing Hong,[2] Martin R. Bryce,*[,1] and Thomas Wandlowski*[,2]

[1] Department of Chemistry, Durham University, Durham DH1 3LE, UK; email: m.r.bryce@durham.ac.uk

[2] Department of Chemistry and Biochemistry, University of Bern, Freiestrasse 3, CH-3012, Bern, Switzerland; email: Thomas.wandlowski@dcb.unibe.ch

Abstract

The synthesis is reported of a new series of olig(oaryleneethynylene) (OAE) derivatives of up to *ca*. 6 nm molecular length (**OAE9**) using iterative Pd-mediated Sonogashira cross-coupling methodology. The oligo-*p*-phenyleneethynylene (OPE) cores of the molecular wires are functionalized at both termini with pyridyl units for attachment to gold leads. The molecular structures determined by single crystal X-ray analysis are reported for **OAE4**, **5**, **7** and **8a**. The charge transport characteristics of derivatives **OAE3 – OAE9** in single-molecular junctions have been studied using the mechanically controlled break junction (MCBJ) technique. The data demonstrate that the junction conductance decreases with increasing molecular length. A transition from coherent transport via tunneling to a hopping mechanism is found for OAE wires longer than ca. 3 nm.

Keywords: Molecular electronics; synthesis; oligomer; oligo(aryleneethynylene); single-molecule conductance; tunneling; hopping

Introduction

Molecular electronics[1,2,3,4,5] is receiving renewed interest due to the intrinsic limitations of silicon-based electronics.[6] Synthetic chemistry has tailored organic molecules to achieve specific electronic functions, even at the single-molecule level.[7,8] Terminal anchor groups which have an affinity for gold are attached to the molecules to achieve the *in situ* assembly of metal–molecule–metal junctions.[9,10,11] The electrical conductance of these nanoscale junctions is characterized using a range of techniques, notably, scanning tunneling microscopy (STM)[12,13] conductive-probe atomic force microscopy (CP-AFM),[14,15] scanning tunneling microscopy break junctions (STM-BJs)[16,17,18] and mechanically controlled break junctions (MCBJs).[19,20,21]

Studies which aim to understand how charge transport mechanisms vary with changing the length of the molecular wire[22,23] have been very limited due to the challenges posed by the synthesis, rigorous purification and measurement of long molecules anchored between two electrodes. Two distinct charge transport mechanisms have been predicted theoretically and identified experimentally: coherent transport via tunneling or superexchange which dominates in short molecules, and incoherent thermally activated hopping in long molecules.[24] Choi et al. reported a series of oligophenyleneimine (OPI) molecules of length ca. 1.5–7 nm with an anchored thiol unit at one terminus and a phenyl unit at the other terminus. Contacting a monolayer of the molecules assembled on gold with a CP-AFM tip revealed a transition from tunneling to hopping at a molecular length of ca. 4 nm in junctions made of hundreds of molecules.[25] Single-molecule measurements were not reported in these studies. Hines et al. reported a transition from tunneling to hopping at a molecular length between 5.2 and 7.3 nm by means of STM-BJ measurements (at the single-molecule level) on four oligofluorene-based molecular wires terminated with thiols.[26]

Oligo(phenyleneethynylene) (OPE) derivatives are ideal candidates for studies on the correlation of conductance with molecular length. They are highly conjugated, rigid, rod-like molecules whose functional properties can be systematically tuned by chemical synthesis, which makes them a very important class of molecules in materials chemistry and molecular electronics.[27,28] Short derivatives, typically OPE3 systems, have been widely studied in metal–molecule–metal junctions,[29,30,31] but there are very few reports of transport studies through longer derivatives.[32] Lu et al. studied a series of OPEs of lengths ca. 1–5 nm with amino groups at both termini and probed the charge transport mechanism in monolayers using STM-BJ and CP-AFM methods. A transition from tunneling to hopping was observed at a molecular length of ca. 2.75 nm.[33] Studies on related derivatives incorporating a ferrocene unit in the backbone, using the same contacting techniques, established that ferrocene enhanced the conductance in both the tunneling and hopping regimes.[34] Single-molecule measurements were not reported in these studies.[33,34]

Terminal 4-pyridyl (PY) units anchor molecules effectively to gold substrates and, unlike thiols,[35,36] they are stable under ambient conditions and no protecting group is needed.[37,38,39,40] We have shown that for tolane derivatives pyridyl exhibits excellent anchoring performance with high conductance and 100% of molecular junctions formed.[41] Therefore, pyridyl units are used as anchors in the present series of molecules, in preference to amine or thiol analogs.

The motivation for this work is to study the length dependence of the *single-molecule* conductance of oligoaryleneethynylene (OAE) derivatives comprising OPE cores terminated at both ends with pyridyl groups. This study is clearly distinct from previous work on OPI[25] and OAE[33,34] derivatives which concerned monolayers comprising hundreds of molecules in closely packed arrangements. The benefit

of single-molecule studies is that artifacts arising from intermolecular interactions (e.g. π–π stacking) which are well-known in OAE derivatives[27] are absent. We describe the synthesis and characterization of derivatives **OAE3–OAE9** of molecular length (i.e. intramolecular N…N distance) ca. 2–6 nm. The charge transport characteristics of these OAE derivatives in single-molecular junctions have been studied using the MCBJ technique in solution and under environmentally controlled conditions.

Results and Discussion

Synthesis

The OAE derivatives studied in this work are shown in Chart 1. The synthetic strategy uses iterative Pd-catalyzed Sonogashira cross-coupling reactions[42] of new, linearly-conjugated phenyleneethynylene building blocks. The retrosynthetic disconnections of the molecules are based on: (i) commercial availability of starting materials; (ii) high yielding reactions; (iii) the synthesis of intermediate reagents which could be easily purified, thereby facilitating the final step to the target OAE derivatives. For the derivatives **OAE4**–**OAE9** hexyloxy substituents are attached to the inner phenyl rings to give the molecules good solubility in organic solvents. Two **OAE3** derivatives were studied (**OAE3a** and **OAE3b**) to confirm that alkoxy substituents do not affect the conductance behavior, as was reported previously for thiol terminated OPE3 analogs.[30] Two **OAE8** derivatives were synthesized: **OAE8a** has only very limited solubility and although an X-ray crystal structure was obtained it could not be purified to the required level for conductance measurements. Analog **OAE8b** with additional hexyloxy sidechains in the backbone has improved solubility and was fully characterized. A key aspect of our strategy is the use of 2-hydroxypropyl protecting groups for the intermediate terminal alkynes, e.g. compounds **2** and **5** (Scheme 1). A benefit of this protecting group (compared to trialkylsilyl, which is more commonly used)[28] is that its high polarity facilitates the separation of any unreacted starting material or byproducts which do not contain this unit. Deprotection with loss of acetone is easily accomplished using sodium hydroxide in toluene.[43] A notable feature of the deprotection reactions is that for bis-protected derivatives **2** and **5**, the major product can be exclusively mono-deprotected (**2→3**) or bis-deprotected (**5→6**) depending on the temperature and the length of time of the reaction. As representatives of the series, the syntheses of **OAE4** and **OAE9** are shown in Scheme 1, and **OAE5** in Scheme 2. The syntheses of the other OAEs are described in the Supporting Information. All the OAE derivatives were characterized by ^{1}H NMR, ^{13}C NMR and mass spectra which confirmed their expected structures and established their high level of purity. Single crystal X-ray structures obtained for **OAE4**, **OAE5**, **OAE7** and **OAE8a** give the molecular lengths and solid-state conformations of the molecules. UV-visible absorption spectra in solution (Table 1) show that for **OAE3-OAE9** there is extended conjugation throughout the backbone and the saturation length has not been reached in the present

series. These crystallographic and spectroscopic characterization data are discussed in detail in the Supporting Information.

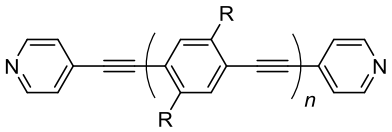

OAE3a *n* = 1; R = H
b *n* = 1; R = OMe
OAE4 *n* = 2; R = OC_6H_{13}
OAE5 *n* = 3; R = OC_6H_{13}

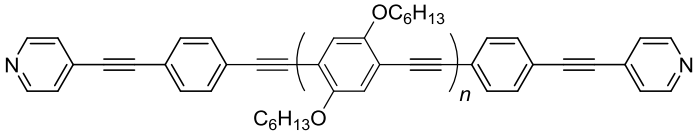

OAE6 *n* = 2
OAE7 *n* = 3

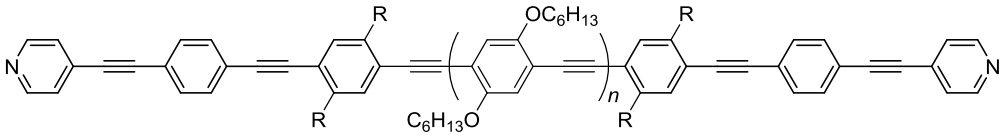

OAE8a *n* = 2; R = H
b *n* = 2; R = OC_6H_{13}
OAE9 *n* = 3; R = OC_6H_{13}

Chart 1. Structures of the OAE derivatives studied in this work.

Scheme 1. Synthesis of **OAE4** and **OAE9**.

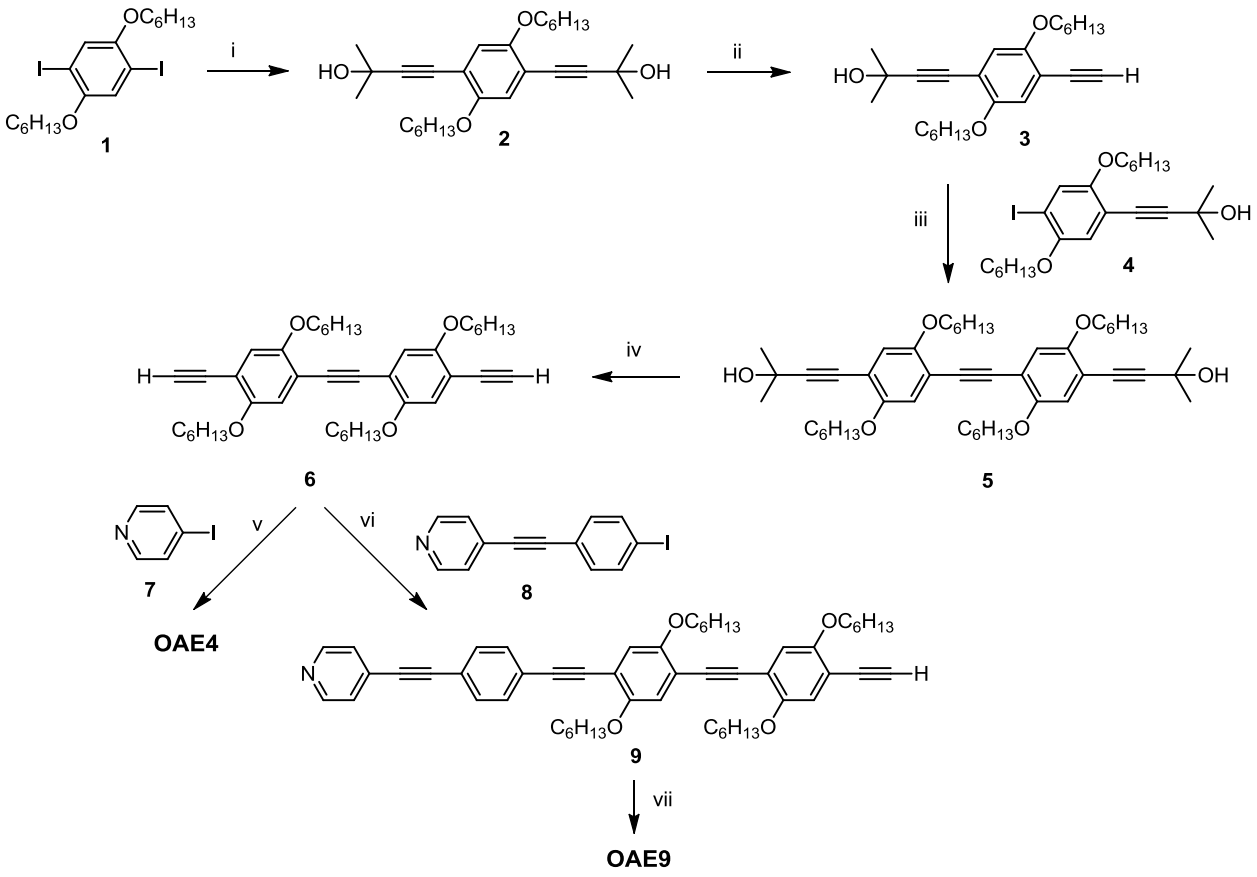

Reagents and conditions: (i) 2-methyl-3-butyn-2-ol, $[PdCl_2(PPh_3)_2]$, CuI, $(i\text{-Pr})_2NH$, 20 h, 20 °C, 95% yield; (ii) NaOH, toluene, 6 h, 70 °C, 65% yield; (iii) **4**, $[Pd(PPh_3)_4]$, CuI, THF, Et_3N, 18 h, 50 °C, 95% yield; (iv) NaOH, toluene, 22 h, 100 °C, 36% yield; (v) **7**, $[Pd(PPh_3)_4]$, CuI, THF, Et_3N, 23 h, 20 °C, 88% yield; (vi) **8**, $Pd[PPh_3]_4$, CuI, THF/Et_3N, 18 h, 20 °C, 60% yield; (vii) **7**, $[Pd(PPh_3)_4]$, CuI, THF, Et_3N, 15 h, 20 °C, 21% yield.

Scheme 2. Synthesis of **OAE5**.

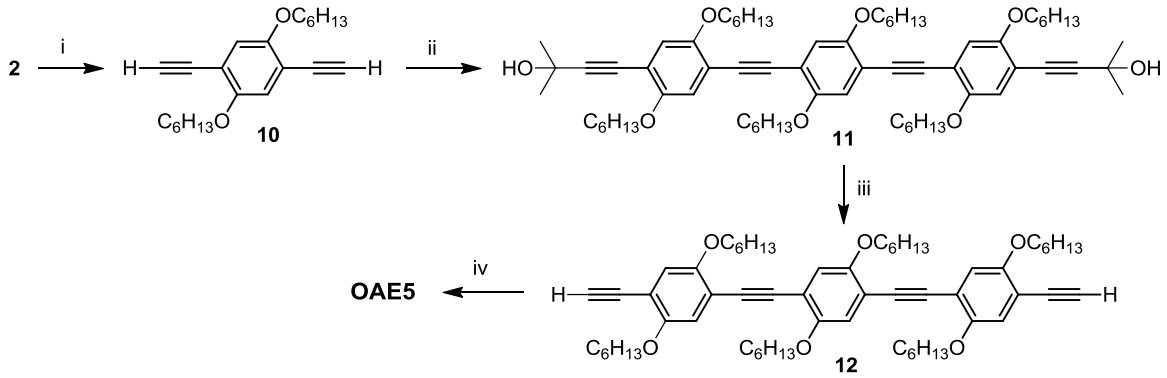

Reagents and conditions: (i) NaOH, toluene, 12 h, 100 ^{o}C, 82% yield; (ii) **3**, [Pd(PPh$_3$)$_4$], CuI, THF, Et$_3$N, 18 h, 20 ^{o}C, 47% yield; (iii) NaOH, toluene, 23 h, 100 ^{o}C, 70% yield; (iv) **7**, [Pd(PPh$_3$)$_4$], CuI, THF, Et$_3$N, 20 h, 20 ^{o}C, 68% yield

Conductance Measurements

The charge transport characteristics of the derivatives **OAE3–OAE9** in single-molecular junctions were investigated using the mechanically controlled break junction (MCBJ) technique. Key parameters are listed in Table 1. Molecular junctions were formed by opening and closing a nanogap between two gold electrodes in a solution of 1,3,5-trimethylbenzene (TMB) and tetrahydrofuran (THF), 4 : 1 (v/v) containing typically 0.1 mM of the target molecules. Details of the experimental set-up were described in our previous publications,[41,44] and are briefly summarized in the Experimental Section.

Table 1. Characteristic parameters of the UV/Vis absorption and transport measurements

Molecule	λ_{max}/nm[a]	L/nm[b]	G^*/G_0 1D[c]	G/G_0 2D[d]	Δz^*[e]	z^*[f]	JFP/%[g]
OAE3a	319	1.6	$10^{-4.5}$	$10^{-5.0}$ - $10^{-4.0}$	1.08	1.58	100
OAE3b	306, 372	1.6	$10^{-4.5}$	$10^{-5.0}$ - $10^{-4.0}$	1.00	1.50	100
OAE4	320, 401	2.3	$10^{-5.5}$	$10^{-6.0}$ - $10^{-5.0}$	1.88	2.38	100
OAE5	324, 417	3.0	$10^{-6.7}$	$10^{-7.0}$ - $10^{-6.2}$	1.92	2.42	71
OAE6	331, 409	3.7	$10^{-6.8}$	$10^{-7.3}$ - 10^{-6}	2.22	2.72	18
OAE7	339, 428	4.4	$10^{-6.9}$	$10^{-7.0}$ - $10^{-6.5}$	2.31	2.81	18
OAE8b	335, 435	5.1	$10^{-6.8}$	$10^{-7.2}$ - 10^{-6}	1.78	2.28	20
OAE9	335, 439	5.8	$10^{-6.9}$	$10^{-7.5}$ - 10^{-6}	1.36	1.86	17

[a] Maxima of the characteristic UV/Vis absorption in CH_2Cl_2 solution; [b]molecular length L, which is defined as the distance between the center of the nitrogen anchor atom at one end of a fully extended isolated molecule to the center of the anchor atom at the other end. The lengths of the molecules were calculated by

ACD/ChemSketch and are in very close agreement with the N…N distances obtained by single-crystal X-ray diffraction for **OAE4**, **5**, **7** and **8a** (see SI). [c] Most probable molecular junction conductance as estimates from Gaussian fits to the experimentally obtained 1D conductance histograms. [d] Conductance range of molecular junctions extracted from the 2D conductance vs. relative displacement histograms. [e] Δz^* as most probable relative junction elongation (displacement); [f] $z^* = \Delta z^* + 0.5$ as absolute junction elongation (displacement), [g] JFP is the junction formation probability.

Figure 1 displays typical conductance (G) versus distance (Δz) stretching traces, as plotted in a semilogarithmic scale, and recorded for 0.1 mM **OAE4** or **OAE7** in TMB/THF using the MCBJ technique. For reference, we also plotted two traces (black curves) representing the OAE-free solution, which reveal classical tunneling characteristics, i.e. an exponential decrease of the conductance upon junction elongation. The traces recorded for **OAE4** and **OAE7**, which are characteristic representatives of the studied pyridyl-terminated OAE family, are more complex. After the formation of the contact between the two gold leads, the nanoscale constriction was stretched with a typical rate of 2 nm s^{-1}. All curves show initially a step-like decrease of the conductance from 10 G_0 up to 1 G_0, with $G_0 = 2e^2/h$ being the fundamental quantum conductance. Opening the gap results in an elongation of the gold-gold junction and decreases the number of gold atoms in the constriction, which causes the conductance to change up to 1 G_0, where the contact between the two gold leads in the MCBJ consists of only one gold atom. Subsequently, an abrupt decrease of the conductance over several orders of magnitude up to 10^{-5} G_0 occurs, which is assigned to the "jump out of atomic contact". [45] The gold-gold contact breaks, and OAE molecules from the solution or already adsorbed at one of the two metal leads bridge the gap. This process is reflected in additional features in the $\log(G/G_0)$ vs. Δz stretching traces. The examples plotted in Figure 1 show well-developed plateaus at $G < 10^{-5}G_0$. These plateaus represent stable molecular junctions "electrode–OAE–electrode". We notice that these traces show a distinct monotonic decrease in the conductance with stretching distance. Upon further pulling, a second decrease in conductance occurs, which is assigned to the rupture of the contact between molecular wire and the gold leads.[31,46] The conductance finally reaches the noise level of $G \leq 10^{-8}G_0$ upon the complete breaking of the molecular junction. We note that the plateau length increases with molecular length L as illustrated in Figure 1 for **OAE4** and **OEA7** as typical examples. We also observed that rupture of the molecular junction is less steep for junctions formed with the longer OAE molecules. The overall shape of the stretching traces as recorded for each molecule is qualitatively similar, but varies in detail. Therefore, a careful statistical analysis of a large number of individual traces is required to extract representative results.

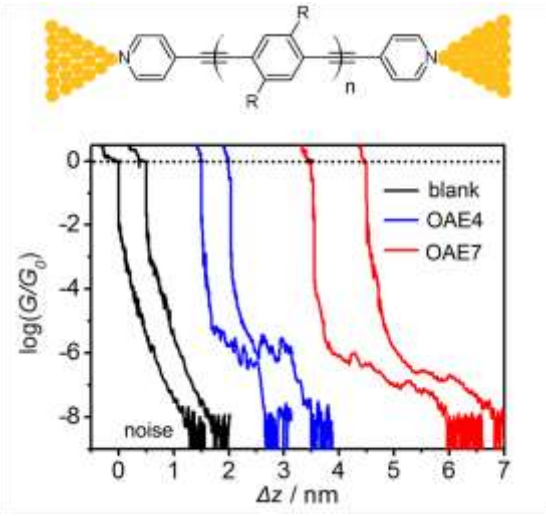

Figure 1. Typical conductance vs. distances traces recorded in TMB/THF in the absence (black lines) and in the presence of 0.1 mM **OAE4** (blue lines) or **OAE7** (red lines) in a MCBJ set-up at 0.10 V bias voltage, stretching rate 2 nm s^{-1}.

Several thousands of individual conductance versus relative displacement traces (G vs. Δz) were recorded and analyzed further by constructing all-data-point histograms without any data selection to extract statistically significant results from the different junction configurations. Figure 2 displays the corresponding one-dimensional (1D) histograms of eight OAEs in a semi-logarithmic scale as constructed from 2000 experimental conductance versus distance traces for each compound. The sharp peaks around 1 G_0 represent the conductance of a single atom gold−gold contact. The prominent peaks between 10^{-7} G_0 < G/G_0 < 10^{-4} G_0 represent molecular features. The 1D histograms reveal one pronounced molecular feature for each OAE derivative. The conductance peaks at $G < 10^{-7.5}$ G_0, which were also observed in OAE-free solutions, are caused by instrumental noise.[41,44] The statistically most probable conductances of molecular junctions formed by the respective OAEs as trapped between two gold contacts were obtained by fitting Gaussians to the characteristic maxima in the conductance histograms. The results are compiled in Table 1. The data presented in Figures 2 and 3 are summarized in Figure 4. We note that rather similar conductance values were found for molecular concentrations ranging between 10^{-6} M up to 10^{-4} M, which supports their assignment to single-molecular junction conductances. The single junction conductances decrease with increasing molecular length L from $10^{-4.5}$ G_0 for **OAE3** to $10^{-6.7}$ G_0 for **OAE5**, by three orders of magnitude. However, this trend levels off for longer molecular wires. The junction conductances of **OAE5** to **OAE9** reveal rather small changes spanning from $10^{-6.7}$ to $10^{-6.9}$ G_0, respectively. We also note that the width of the molecular conductance features increases with molecular length, which most probably reflects the increasing number of molecular conformations in the nanoscale junctions.

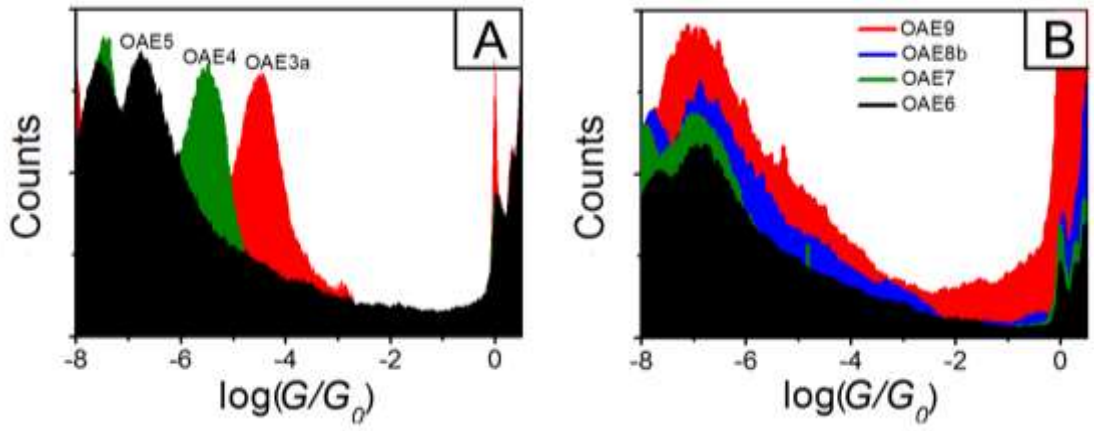

Figure 2. All-data point 1D conductance histograms of OAE-derivatives as constructed from 2000 individual conductance vs. relative distance traces as plotted in Figure 3.

The above analysis was extended by constructing two-dimensional (2D) conductance vs. relative displacement Δz histograms. Figures 3A and 3B show typical results for **OAE4** and **OAE7**. The corresponding graphs of the other molecules are summarized in the Supporting Information. The 2D conductance histograms were obtained as follows.[41,47,48] First we normalized all individual conductance traces to a common distance scale by assigning the relative displacement $\Delta z = 0$ at $G = 0.7\ G_0$. This procedure is justified by the sharp drop in conductance around 1 G_0. The conductance versus relative displacement histogram was then constructed by counting the occurrences of [log(G/G_0), Δz] pairs in a 2D field. The 2D histograms of **OAE4** and **OAE7** show features of gold quantum contacts around $G \geq 1G_0$ and a second cloud-like pattern in [0.5 nm < Δz < 1.8 nm, $10^{-6.2}\ G_0 < G < 10^{-4.8}\ G_0$] centered at $G = 10^{-5.5}\ G_0$ (**OAE4**) and in [0.5 nm < Δz < 2.2 nm, $10^{-7.0}\ G_0 < G < 10^{-6.5}\ G_0$] centered at $G = 10^{-6.9}\ G_0$ (**OAE7**). We attribute the latter to the formation of single-molecule junctions. The corresponding characteristic conductance data are rather close to the positions of conductance peaks in the 1D histograms. Similar conclusions were also obtained for the other OAE derivatives (see Supporting Information). We also note that all 2D conductance histograms reveal a small but distinct decrease of the single junction conductance G with increasing displacement Δz. The corresponding intervals are given in Table 1 for all the compounds investigated. Finally, we comment that the data cloud below $10^{-7.5}\ G_0$ represents the noise level.

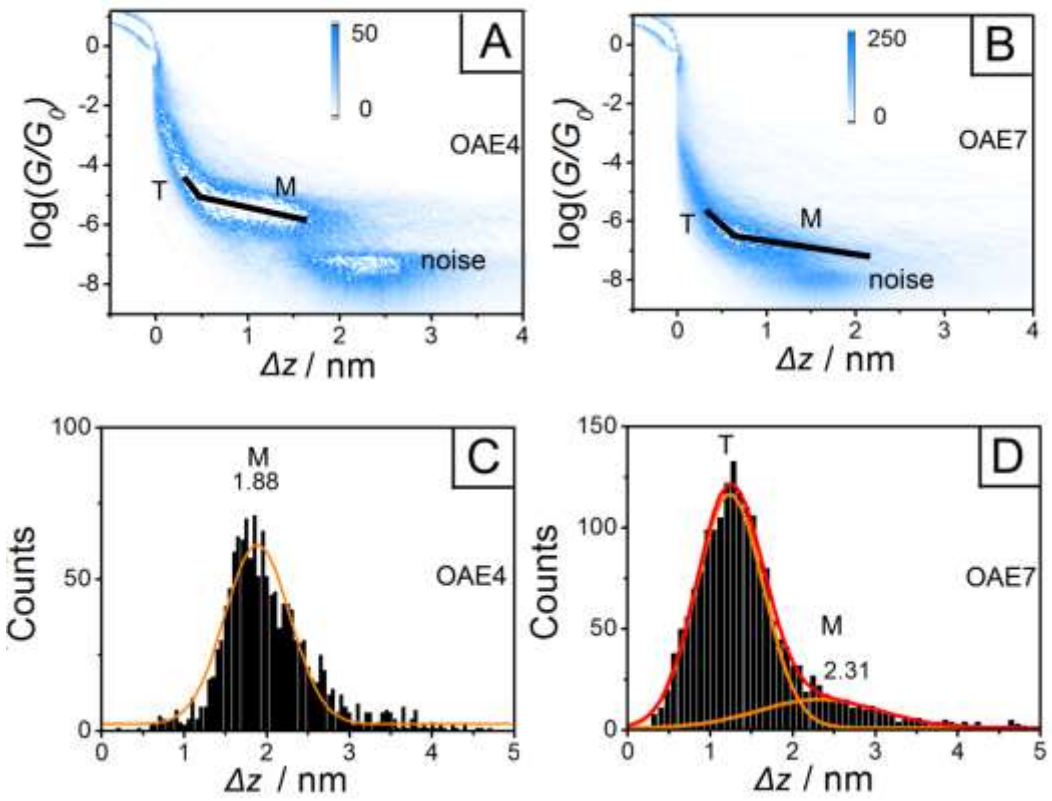

Figure 3. (A,B) 2D conductance-relative-displacement histograms from MCBJ-BJ experiments for **OAE4** (A) and **OAE7** (B). (C,D) Relative displacement (*Δz)* distribution from MCBJ-BJ experiments for **OAE4** (C) and **OAE7** (D). The relative displacement histograms are obtained from conductance traces between 0.1 G_0 and 10^{-7} G_0. The envelope traces represent Gaussian fits to the molecular junction contribution and to direct tunnelling, labelled as M and T, respectively.

Analyzing the evolution of a molecular junction upon stretching provides additional information about the stability and junction formation probability. We constructed relative displacement (*Δz*) histograms[41] by calculating the displacement from the relative zero position at 0.7 G_0 to the end of the molecular conductance region, just before the onset of the noise level. Figures 3C and 3D display characteristic displacement histograms of **OAE4** and **OAE7**. The plot of **OAE4** reveals a uniform normal distribution with a well-defined maximum. No stretching traces shorter than 1.2 nm were observed indicating that no significant contribution due to direct tunnelling (T) through the solution exists. Therefore, we conclude that the molecular junction formation probability of **OAE4** approaches 100%. The single maximum in Figure 3C represents the most probable relative characteristic stretching distance *Δz** = 1.88 nm, which may be considered as a measure of the most probable characteristic plateau length of an **OAE4**-type molecular junction.[41] The most probable absolute displacement *z** in

an experimental molecular junction formed between two gold tips and **OAE4** is obtained by adding the snap-back distance Δz_{corr} to the relative displacement: $z^* = \Delta z^* + \Delta z_{corr}$. Referring to our previous work with pyridyl-terminated rigid rod-like tolanes we used $\Delta z_{corr} = (0.5 \pm 0.1)$ nm,[41] which leads to $z^* = 2.38$ nm for **OAE4**. (This value is close to the molecular length L of **OAE4**.) Similar trends were found with **OAE3** (c.f. data in Table 1).

The 1D displacement histograms of the longer OAEs are more complex. Figure 3D illustrates data of **OAE7** as an example. In addition to a well-developed molecular feature with a maximum at $\Delta z^* = 2.31$ nm, which gives $z^* = 2.81$ nm as the most probable absolute displacement, we observed a second peak with a maximum around 1.2 nm. This peak originates from an increasing number of individual conductances versus distance traces without the formation of a molecular junction. In other words, it represents contributions from direct tunneling. The area ratio between the molecular contribution and the total data density in the histogram plotted in Figure 3D leads to a junction formation probability of 18% for **OAE7**. A similar analysis of our experiments with **OAE6** and **OAE9** reveals the following trends: (i) The molecular junctions break prior to a fully extended configuration; (ii) the molecular features in the 1D displacement histograms broaden and (iii) the junction formation probability decreases considerably with increasing molecular length L. These observations demonstrate that the larger number of molecular conformations and/or the increasing number of hexyloxy side-chains of the longer OAEs appear to hamper the formation of stable (single) molecular junctions. Changes in the molecular structure near the pyridyl binding site may play a role. For **OAE3**–**OAE5** the phenyl rings adjacent to the pyridyls are disubstituted with alkoxy groups, whereas for **OAE6–OAE9** these rings are unsubstituted. The latter might strengthen the π–interaction of the molecule with the gold substrate, and therefore, an additional energy might be needed to lift the respective OAEs from the substrate surface. This extra energy threshold might not always be reached, so that the percentage of stretching events which are unsuccessful (no molecular junctions being formed) is larger, which leads to lower junction formation probability. This process is currently being studied by molecular dynamics simulations in combination with electromechanical force–distance and conductance–distance measurements. However, this topic is beyond the scope of this article.

Figure 4 displays the dependence of the most probable single junction conductances of the pyridyl-terminated OAE family on molecular length L. We found two distinctly different regions. For the shorter molecules, from **OAE3** to **OAE5**, the conductance decreases exponentially according to eqn. 1 [23,31]

$$G = G_c e^{-\beta L}$$

with an attenuation constant β = (3.3 ± 0.1) nm^{-1} and a contact conductance per pyridyl terminating group, G_c = (0.54 ± 0.07) μS at L = 0, which leads to a contact resistance $R_c = 1/G_c$ = (1850 ± 232) kΩ. Similar values of β were reported for other rigid-rod-like single molecular wires or assembled monolayers, such as dithiol-terminated OPEs (3.4 ± 0.1 nm^{-1}),[31] oligophenyleneimines (OPI, β = 3.0 nm^{-1}),[25] oligophenylenedithiols (PP, β = (3.5 – 5.0) nm^{-1})[49,50] or pyridyl-terminated oligoynes (OY, β =(3.1 ± 0.4) nm^{-1}).[51] Smaller values of β were reported for OPEs with amine anchoring groups (OPE, β = 2.0 nm^{-1})[33], oligoflourenes (OF, β = (2.06 ± 0.09 nm^{-1})),[26] oligophenylene-vinylenes (OPV, β = (1.7 – 1.8) nm^{-1}),[46,52] oligothiophenes (OT, β = ~1 nm^{-1})[53] as well as for metal-porphyrin containing molecular wires (P, β <<0.1 nm^{-1}).[54]

The contact resistance R_c = 1850 kΩ per pyridyl anchoring group for the family of OAE-wires studied in this work is larger than R_c = 205 kΩ, which is the corresponding value for pyridyl-terminated oligoynes.[51] A similar trend is observed with the dithiol-terminated OPEs (40 kΩ)[31] and oligoynes (~ 3.2 kΩ).[51] These data demonstrate that the values are not only determined by the molecular anchoring site but also by the coupling of the anchor group to the wire backbone.

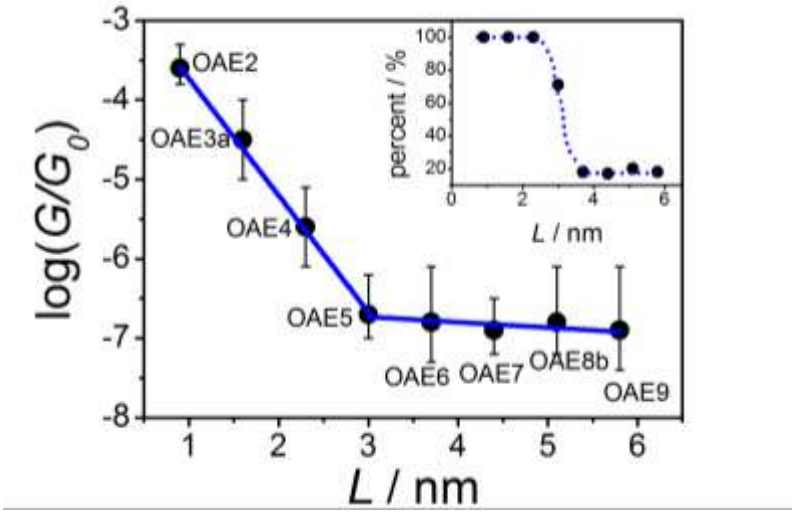

Figure 4. Semi-logarithmic plot of the most probable single molecule junction conductances (individual data points as obtained from the analysis of the 1D conductance histograms) and of the conductance range (bare symbols as extracted from the analysis of the 2D conductance histograms) in units of log(G/G_0) versus the molecular length for a family of pyridyl-terminated OAE derivatives. The inset represents the junction formation probability (JFP) in dependence on the molecular length L. All numerical data are compiled in Table 1.

Comparing the results of the single-molecule conductance measurements for the short OAEs **OAE3** - **OAE5** with the literature data above, and in particular with results reported for pyridyl-terminated oligoynes[51] and thiol-terminated OPEs,[31] as well as the excellent fit of eqn. 1 to the experimental data, demonstrates that electron transport across the **OAE3** to **OAE5** wires is controlled by coherent transport via tunneling or superexchange.

A distinctly different behavior is found for the longer derivatives **OAE6** to **OAE9**. The most probable single junction conductances are still exponentially dependent on molecular length *L*. However, the fit of eqn. 1 to the experimental data gives an attenuation constant β = (0.16 ±0.08) nm^{-1}, which is significantly smaller as compared to the β = (3.3 ±0.01) nm^{-1}, the values extracted from the analysis of the shorter **OAE**s. Similar small β values were reported for longer amine-terminated OPEs ($\beta \sim 0.3\ nm^{-1}$),[33] thiol-terminated oligofluorenes ($\beta << 0.1\ nm^{-1}$)[26] and longer oligophenylenimines ($\beta \sim 0.9\ nm^{-1}$).[23] Comparing these results suggests that transport through the longer pyridyl-terminated OAEs is characterized by a thermally activated hopping mechanism.[24] Transition from tunneling to hopping was found at a molecular length of ~ 3 nm for the present system.

Single-molecule studies of length dependence have not been reported previously for OAE systems. CP-AFM experiments, which involve contacting hundreds of molecules within self-assembled monolayers, revealed the transition from tunnelling to hopping at a molecular length of ca. 2.75 nm for a series of amine-terminated OPEs[33] and ca. 4 nm for thiol-anchored oligophenyleneimines.[25] Single-molecule conductance experiments employing the STM-BJ techniques reported characteristic transition lengths of 5.6 to 6.8 nm for polythiophenes[55] and 5.2 to 7.3 nm for oligofluorene-based molecular wires,[26] both terminated with thiol anchors. We note that for the oligofluorene series the experiments are very limited within the length range investigated.[26] This comparison demonstrates convincingly that the transition length from tunneling to transport controlled by hopping depends critically on the structure of the molecular backbone. However, the existing limited data-base of single molecular junction studies does not yet allow general trends to be extracted. Comparative studies with well-defined molecular wires, not only of known and tunable length but in particular of molecular conformation, are essential to achieve this goal.

Conclusions

We have presented the synthesis of a family of new linear OAE derivatives with terminal pyridyl anchor groups of molecular length ca. 2 – 6 nm. The charge transport properties of these molecular wires were characterized by MCBJ experiments. Single-molecule junction conductance measurements reveal a transition from coherent transport via tunnelling, which dominates in shorter molecules, to an

incoherent hopping in longer molecules. The transition occurs at a molecular length L ~ 3.0 nm and for conductances below $10^{-6.5}$ G_0. Increasing the molecular length L leads also to a reduction of the probability for molecular junction formation from 100% to values below 20%. This trend is attributed to the larger number of molecular conformations and the increasing number of hexyloxy side-chains, which appear to hamper the formation of stable OAE-type (single) molecular junctions. A comparison of our data with literature data for other oligomer systems establishes that the details of the tunneling to hopping transition depend on the nature of the molecular wire backbone as well as its coupling to the respective anchoring sites. This work represents the first studies on length dependence of conductance of OAE derivatives at the single-molecule level. However, unambiguous and more general correlations between structure and transport characteristics cannot yet be established due to the limited number of reliable single junction conductance studies with long molecular wires of well-defined structure, in particular molecular conformation. This topic comprises a major challenge for future research in synthetic and materials chemistry.

Experimental Section

Characterization data for the OAE Derivatives

OAE3a was synthesized following the literature route and the characterization data are in agreement with those reported.[40]

OAE3b. m.p. 189.1-190.2 ^{o}C. ^{1}H NMR (400 MHz, $CDCl_3$) δ 8.63 (dd, J = 4.5, 1.6 Hz, 4H), 7.44 (dd, J = 4.5, 1.6 Hz, 4H), 7.07 (s, 2H), 3.94 (s, 6H); ^{13}C NMR ($CDCl_3$, 101 MHz): 154.57, 150.04, 131.49, 125.72, 116.19, 113.63, 92.71, 90.21, 56.78; MS (ASAP+) *m/z* : 508.2 (M^+, 100%).

OAE4. m.p. 107.0-107.5 °C. ^{1}H NMR (700 MHz, $CDCl_3$) δ 8.60 (d, *J* = 5.6Hz, 4H), 7.37 (d, *J* = 5.6Hz, 4H), 7.02 (s, 2H), 7.01 (s, 2H), 4.03 (m, 8H), 1.84 (m, 8H), 1.52 (m, 8H), 1.34 (m, 16H), 0.89 (m, 12H); ^{13}C NMR (151 MHz, $CDCl_3$) δ 153.98, 153.45, 149.61, 131.69, 125.41, 117.14, 116.96, 115.33, 112.66, 91.94, 91.75, 90.80, 69.74, 69.51, 31.58, 31.54, 29.25, 29.23, 25.71, 25.64, 22.62, 14.01, 13.99; HR-MS (ASAP+) *m/z* Calcd for $C_{52}H_{65}N_2O_4$ $[M+H]^+$ 781.4944, found *m/z*: $[M+H]^+$ 781.4937.

OAE5. m.p. 127.2-128.2 °C. ^{1}H NMR (700 MHz, $CDCl_3$) δ 8.59 (d, *J* = 5.7 Hz, 4H), 7.36 (d, *J* = 5.7 Hz, 4H), (7.01 (m, 6H), 4.02 (m, 12H), 1.84 (m, 12H), 1.51 (m, 12H), 1.33 (m, 24H), 0.88 (m, 18H); ^{13}C NMR (176 MHz, $CDCl_3$) δ 153.99, 153.53, 153.41, 149.63, 131.67, 125.40, 117.24, 117.18, 116.95, 115.54, 114.27, 112.49, 92.05, 91.87, 91.31, 90.81, 69.76, 69.66, 69.50, 31.59, 31.58, 31.54, 29.27, 29.24, 29.23, 25.70, 25.66, 25.64, 22.61, 14.00, 13.98; HR-MS (ASAP+) *m/z* Calcd for $C_{72}H_{93}N_2O_6$

$[M+H]^+$ 1081.7034, found *m/z* : $[M+H]^+$ 1081.7070.

OAE6. m.p. 214.2-215.2 °C. ^{1}H NMR (600 MHz, $CDCl_3$) δ 8.62 (bs, 4H), 7.52 (bs, 8H), 7.39 (d, *J*=4.2Hz, 4H), 7.01 (s, 2H), 7.00 (s, 2H), 4.03 (m, 8H), 1.85 (m, 8H), 1.53 (m, 8H), 1.34 (m, 16H), 0.89 (m, 12H); ^{13}C NMR (151 MHz, $CDCl_3$) δ 153.72, 153.49, 149.53, 131.78, 131.54, 131.43, 125.58, 124.44, 121.64, 117.02 (2 overlapping peaks), 114.68, 113.51, 94.30, 93.85, 91.64, 88.61, 88.30, 69.72, 69.55, 31.60, 31.59, 29.30, 29.26, 25.74, 25.65, 22.62, 14.02; HR-MS (ASAP+) *m/z* Calcd for $C_{68}H_{73}N_2O_4$ $[M+H]^+$ 981.5570, found *m/z* : $[M+H]^+$ 981.5566.

OAE7. m.p. 203.5-204.2 °C. ^{1}H NMR (600 MHz, $CDCl_3$) δ 8.61 (d, *J* = 6.0 Hz, 4H), 7.52 (s, 8H), 7.39 (d, *J* = 6.0 Hz, 4H), 7.01 (m, 3H), 4.03 (m, 12H), 1.84 (m, 12H), 1.52 (m, 12H), 1.34 (m, 24H), 0.89 (m, 18H); ^{13}C NMR (151 MHz, $CDCl_3$) δ 153.73, 153.50, 153.47, 149.49, 131.79, 131.54, 131.50, 125.55, 124.47, 121.61, 117.23, 117.04, 117.01, 114.78, 114.28, 113.42, 94.26, 93.92, 91.78, 91.45, 88.64, 88.27, 69.73, 69.67, 69.54, 31.61, 31.59, 29.30, 29.29, 29.26, 25.75, 25.67, 25.65, 22.62, 14.02; HR-MS (ASAP+) *m/z* Calcd for $C_{88}H_{101}N_2O_6$ $[M+H]^+$ 1281.7700, found *m/z* : $[M]^+$ 1281.7615.

OAE8b. m.p. 199.5 -200.6 °C. ^{1}H NMR (600 MHz, $CDCl_3$) δ 8.61 (d, *J* = 5.2 Hz, 4H), 7.53 (s, 8H), 7.38 (d, *J* = 5.2 Hz, 4H), 7.02 (m, 8H), 4.04 (m, 16H), 1.86 (m, 16H), 1.53 (m, 16H), 1.35 (m, 32H), 0.89 (m, 24H). ^{13}C NMR (151 MHz, $CDCl_3$) δ 153.74, 153.52, 153.50, 153.48, 149.72, 131.78, 131.54, 131.26, 125.48, 124.44, 121.67, 117.26, 117.24, 117.06, 117.02, 114.81, 114.40, 114.21, 113.42, 94.28, 93.68, 91.83, 91.61, 91.44, 88.65, 88.34, 69.74, 69.68, 69.66, 69.54, 31.62, 31.61, 31.60, 29.32, 29.30, 29.27, 25.76, 25.68, 25.57, 22.64,14.03. HR-MS (ASAP+) m/z calcd for $C_{108}H_{128}N_2O_8$ $[M]^+$ 1580.9671, found m/z : $[M]^+$ 1580.9725.

OAE9. m.p. 202.1-203.5 °C. ^{1}H NMR (400 MHz, $CDCl_3$) δ 8.62 (d, *J* = 6.0 Hz, 4H), 7.54 (bs, 8H), 7.40 (d, *J* = 6.0 Hz, 4H), 7.02 (m, 10H), 4.03 (m, 20H), 1.86 (m, 20H), 1.53 (m, 20H), 1.34 (m, 40H), 0.89 (m, 30H); ^{13}C NMR (101 MHz, $CDCl_3$) δ 153.95, 153.74, 153.71 (two overlapping peaks), 153.69, 149.91, 132.04, 131.80, 131.59, 125.77, 124.68, 121.89, 117.98, 117.44, 117.22, 115.01, 114.79, 114.61, 114.50, 114.38, 113.61, 112.82, 94.52, 94.01, 92.07, 91.87, 91.80, 91.66, 88.88, 88.56, 69.95, 69.88, 69.75, 31.87, 31.85, 31.78, 29.53, 29.50, 26.00, 25.92, 25.86, 22.89, 14.29. MS ($ASAP^+$) *m/z* : 1883.1 ($[M+H]^+$, 100%).

Mechanically controlled break junction (MCBJ) measurements.

The transport characteristics in single-molecule junctions were studied by MCBJ-measurements in solution at room temperature. The latter contained typically 0.1 mM of the OAE-type molecules in a mixture of 1,3,5-dimethylbenzene (TMB; Aldrich, p.a.) and tetrahydrofuran (THF; Aldrich, p.a), 4:1

(v/v).

The MCBJ experiments are based on the formation and breaking of a nanogap between a notched, freely suspended gold wire (0.1 mm diameter, 99.999%, Goodfellow), fixed on spring steel sheets (10 mm × 30 mm, thickness 0.25 mm) with a two-component epoxy glue (Stycast 2850 FT with catalyst 9). The sample sheets were fixed between two holders. A Kel-F liquid cell with a Kalrez O-ring was mounted onto the sheet. During the measurements, the steel sheet could be bent with a pushing rod, which was controlled by a combination of a stepper motor and a piezo stack. The bending was initialized by the stepper motor. Once the measured current decreased to a value corresponding to 15 G_0 the stepper motor stops to move, and the piezo stack was activated. This strategy reduced significantly noise contributions from the operation of the stepper motor. The movement of the piezo stack controlled the breaking and the reformation of nanoscale contacts, typically in the range between the noise threshold ($G < 10^{-8}\ G_0$) and a high conductance limit, which was set to 10 G_0. Molecular junctions could form upon breaking the gold-gold nanocontacts. The entire cycle was repeated more than 2000 times to obtain statistically relevant data. In the MCBJ setup, the current could be recorded as a feedback signal at a given bias voltage (typically between 0.020 and 0.200 V). The two ends of the "broken wire" were taken as working electrodes WE1 and WE2.

The MCBJ unit is controlled by a lab-built bipotentiostat with two bipolar tunable logarithmic $I - V$ converters as current measuring units, which are operated by a custom-designed micro-controller. The system provides three analog signals: the potential of WE1, the voltage difference between the two working electrodes WE1 and WE2 (bias voltage V_{bias}), driving the current through the two gold electrodes for the conductance measurements, and the voltage output of the piezo stack in the range of 0 to 50 V, allowing the displacement of the piezo stack up to 8 μm with rates ranging from 3 to 3000 nm s^{-1}. The latter translates into lateral pulling (pushing) rates between the two gold leads of 0.1 to 100 nm s^{-1}. The distance between the two gold electrodes in the MCBJ setup was calibrated with complementary STM-BJ experiments assuming that the tunneling decay is identical under the same experimental conditions. Further technical details of the MCBJ set-up reported by Hong et al. in refs. [41,44]

Author Contributions.

$^{\perp}$ These authors contributed equally.

Notes. The authors declare no competing financial interest.

Acknowledgements. X.Z. thanks the China Scholarship Council for a studentship award. The work was

funded by The European Commission (EC) FP7 ITN "FUNMOLS" Project No. 212942.

Supporting Information. Details of molecular synthesis and characterization, X-ray crystallographic data (CCDC 951746 to 951749), UV-vis absorption spectra and single junction conductance measurements. This material is available free of charge through the internet at http://pubs.acs.org.

---

(1) Wassel, R. A.; Gorman, C. B. *Angew. Chem. Int. Ed. Engl.* **2004**, *33*, 5120-5123.

(2) Joachim, C.; Gimzewski, J. K.; Aviram, A. *Nature* **2000**, *408*, 541-548.

(3) Cuevas, J. C.; Scheer, E. *Molecular Electronics: An Introduction to Theory and Experiment*; World Scientific: Singapore, 2010.

(4) Mann, B.; Kuhn, H. *J. Appl. Phys.* **1971**, *42*, 4398-4405.

(5) Aviram, A.; Ratner, M. A. *Chem. Phys. Lett.* **1974**, *29*, 277-283.

(6) Mack, C. A. *IEEE Transactions on Semiconductor Manufacturing* **2011**, *24*, 202-207.

(7) Weibel, N.; Grunder, S.; Mayor, M. *Org. Biomol. Chem.* **2007**, *5*, 2343-2353.

(8) James, D. K.; Tour, J. M. *Aldrichimica Acta* **2006**, *39*, 47-56.

(9) James, D. K.; Tour, J. M. *Chem. Mater.* **2004**, *16*, 4423-4435.

(10) McCreery, R. L. *Chem. Mater.* **2004**, *16*, 4477-4496.

(11) Chen, F.; Hihath, J.; Huang, Z. F.; Li, X. L.; Tao, N. J. *Annu. Rev. Phys. Chem.* **2007**, *58*, 535-564.

(12) Donhauser, Z. J.; Mantooth, B. A.; Kelly, K. F.; Bumm, L. A.; Monnell, J. D.; Stapleton, J. J.; Price, D. W.; Rawlett, A. M.; Allara, D. L.; Tour, J. M.; Weiss, P. S. *Science* **2001**, *292*, 2303-2307.

(13) Repp, J.; Meyer, G.; Paavilainen, S.; Olsson, F. E.; Persson, M. *Science* **2006**, *312*, 1196-1199.

(14) Cui, X. D.; Primak, A.; Zarate, X.; Tomfohr, J.; Sankey, O. F.; Moore, A. L.; Moore, T. A.; Gust, D.; Harris, G.; Lindsay, S. M. *Science* **2001**, *294*, 571-574.

(15) Fan, F. R. F.; Yang, J. P.; Cai, L. T.; Price, D. W.; Dirk, S. M.; Kosynkin, D. V.; Yao, Y. X.; Rawlett, A. M.; Tour, J. M.; Bard, A. J. *J. Am. Chem. Soc.* **2002**, *124*, 5550-5560.

(16) Xu, B. Q.; Tao, N. J. J. *Science* **2003**, *301*, 1221-1223.

(17) Venkataraman, L.; Klare, J. E.; Nuckolls, C.; Hybertsen, M. S.; Steigerwald, M. L. *Nature* **2006**, *442*, 904-907.

(18) Haiss, W.; van Zalinge, H.; Higgins, S. J.; Bethell, D.; Hobenreich, H.; Schiffrin, D. J.; Nichols, R. J. *J. Am. Chem. Soc.* **2003**, *125*, 15294-15295.

(19) Reed, M. A.; Zhou, C.; Muller, C. J.; Burgin, T. P.; Tour, J. M. *Science* **1997**, *278*, 252-254.

(20) Smit, R. H. M.; Noat, Y.; Untiedt, C.; Lang, N. D.; van Hemert, M. C.; van Ruitenbeek, J. M. *Nature* **2002**, *419*, 906-909.

(21) Wu, S. M.; Gonzalez, M. T.; Huber, R.; Grunder, S.; Mayor, M.; Schonenberger, C.; Calame, M. *Nat. Nanotechnol.* **2008**, *3*, 569-574.

(22) Lui, H.; Yu, C.; Gao, N.; Zhao, J. *ChemPhysChem* **2010**, *11*, 1895-1902.

(23) Luo, L.; Choi, S. H.; Frisbie, C. D. *Chem. Mater.* **2011**, *23*, 631-645.

(24) Davis, W. B.; Svec, W. A.; Ratner, M. A.; Wasielewski, M. R. *Nature* **1998**, *396*, 60–63.

(25) S. H. Choi, B. Kim, C. D. Frisbie, *Science* **2008**, *320*, 1482 –1486.

(26) Hines, T.; Diez-Perez, I.; Hihath, J.; Liu, H.; Wang, Z-S.; Zhao, J.; Zhou, G.; Müllen, K.; Tao, N. *J. Am. Chem. Soc*. **2010**, *132*, 11658-11664.

(27) Bunz, U. H. F. *Chem. Rev*. **2000**, *100*, 1605-1644.

(28) Jenny, N. M.; Mayor, M.; Eaton, T. R. *Eur. J. Org. Chem*. **2011**, 4965-4983.

(29) Tour, J. M.; Rawlett, A. M.; Kozaki, M.; Yao, Y.; Jagessar, R. C.; Dirk, S. M.; Price, D. W.; Reed, M. A.; Zhou, C.-W.; Chen, J.; Wang, W.; Campbell, I. *Chem. Eur. J*. **2001**, *7*, 5118-5134.

(30) Huber, R.; Gonzalez, M. T.; Wu, S.; Langer, M.; Grunder, S.; Horhoiu, V.; Mayor, M.; Bryce, M. R.; Wang, C. S.; Jitchati, R.; Schonenberger, C.; Calame, M. *J. Am. Chem. Soc.* **2008**, *130*, 1080–1084.

(31) Kaliginedi, V.; Moreno-García, P.; Valkenier, H.; Hong, W.; García-Suárez, V. M.; Buiter, P.; Otten, J. L. H.; Hummelen, J. C.; Lambert, C. J.; Wandlowski, T. *J. Am. Chem. Soc.* **2012**, *134*, 5262-5275.

(32) Hu, W.; Jiang, J.; Nakashima, H.; Luo, Y.; Kashimura, Y.; Chen, K.-Q.; Shuai, Z.; Furukawa, K.; Lu, W.; Liu, Y.; Zhu, D.; Torimitsu, K. *Phys. Rev. Lett*. **2006**, *96*, 027801.

(33) Lu, Q.; Liu, K.; Zhang, H.; Du, Z.; Wang, X.; Wang, F. *ACS Nano* **2009**, *3*, 3861-3868.

(34) Lu, Q.; Yao, C.; Wang, X.; Wang, F. *J. Phys. Chem. C* **2012**, *116*, 17853-17861.

(35) Tour, J. M.; Jones, L. II.; Pearson, D. L.; Lamba, J. J. S.; Burgin, T. P.; Whitesides, G. W.; Allara, D. L.; Parikh, A. N.; Atre, S. V. *J. Am. Chem. Soc.* **1995**, *117*, 9529-9534.

(36) Valkenier, H. V. H.; Huisman, E. H.; van Hal, P. A.; de Leeuw, D. M.; Chiechi, R. C.; Hummelen, J. C. *J. Am. Chem. Soc.* **2011**, *133*, 4930-4939.

(37) Xu, B. Q.; Tao, N. J. J. *Science* **2003**, *301*, 1221-1223.

(38) Wang, C. S.; Batsanov, A. S.; Bryce, M. R.; Martin, S.; Nichols, R. J.; Higgins, S. J.; Garcia-Suarez, V. M.; Lambert, C. J., *J. Am. Chem. Soc.* **2009**, *131*, 15647-15654.

(39) Kamenetska, M.; Quek, S. Y.; Whalley, A. C.; Steigerwald, M. L.; Choi, H. J.; Louie, S. G.; Nuckolls, C.; Hybertsen, M. S.; Neaton, J. B.; Venkataraman, L. *J. Am. Chem. Soc.* **2010**, *132*, 6817-6821.

(40) Grunder, S.; Huber, R.; Horhoiu, V.; Gonzalez, M. T.; Schoenenberger, C.; Calame, M.; Mayor, M. *J. Org. Chem*. **2007**, *72*, 8337-8344.

(41) Hong, W.; Manrique, D. Z.; Moreno-García, P.; Gulcur, M.; Mishchenko, A.; Lambert, C. J.; Bryce, M. R.; Wandlowski, T. *J. Am. Chem. Soc.* **2011**, *134*, 2292-2304.

(42) Sonogashira, K. *J. Organomet. Chem*. **2002**, *653*, 46.

(43) Dabdoub, M. J.; Dabdoub, V. B.; Lenardão, E. J. *Tetrahedron Lett*. **2001**, *42*, 1807-1809.

(44) Hong, W.; Valkenier, H.; Meszaros, G.; Manrique, D. Z.; Mishchenko, A.; Putz, A.; Garcia, P. M.; Lambert, C. J.; Hummelen, J. C.; Wandlowski, T. *Beilstein Journal of Nanotechnology* **2011**, *2*, 699-713.

(45) Quek, S.Y.; Kamenetska, M.; Steigerwald, M. L.; Choi, H. J.; Louie, S. G.; Hybertsen, M. S.; Neaton, J. B.; Venkataraman, L. *Nature Nanotechnol.* **2009**, *4*, 230-234.

(46) Newton, M. D; Smalley, J. F. *Phys. Chem. Chem. Phys.* **2007**, 9, 555-572.

(47) Mishchenko, A.; Zotti, L. A.; Vonlanthen, D.; Burkle, M.; Pauly, F.; Cuevas, J. C.; Mayor, M.; Wandlowski, Th. *J. Am. Chem. Soc.* **2011**, *133*, 184-187.

(48) Martin, C. A.; Ding, D.; Sorensen, J. K.; Bjornholm, T.; van Ruitenbeek, J. M.; van der Zant, H. S. J. *J. Am. Chem. Soc.* **2008**, *130*, 13198-13199.

(49) Wold, D. J.; Haag, R.; Rampi, M. A.; Frisbie, C. D. *J. Phys. Chem. B* **2002**, 106, 2813-2816.

(50) Ishida, T.; Mizutani, W.; Aya, Y.; Ogiso, H.; Sasaki, S.; Tokumoto, H. *J. Phys. Chem. B* **2002**, 106, 5886-5892.

(51) Moreno-García, P.; Gulcur, M.; Manrique, D. Z.; Pope, Th.; Hong, W.; Kaliginedi, V.; Huang, C.; Batsanov, A. S.; Bryce, M. R.; Lambert, C.; Wandlowski, Th. *J. Am. Chem. Soc*. **2013**, *135*, 12228-12240.

(52) Liu, H.; Wang, N.; Zhao, J.; Guo, Y.; Yin, X.; Boey, F. Y. C.; Zhang, H. *ChemPhysChem* **2008**, *9*, 1416-1424.

(53) Yamada, R.; Kumazawa, H.; Noutoshi, T.; Tanaka, S.; Tada, H. *Nano Lett.* **2008**, *8*, 1237-1240.

(54) Sedghi, G.; Garcia-Suarez, V. M.; Esdaile, L. J.; Anderson, H. L.; Lambert, C. J.; Martin, S.; Bethell, D.; Higgins, S. J.; Elliott, M.; Bennett, N.; Macdonald, E. J.; Nichols, R. J. *Nature Nanotechnology* **2011**, *6*, 517-523.

(55) Yamada, R.; Kumazawa, H.; Tanaka, S.; Tada, H. *Appl. Phys. Express* **2009**, *2* (2), 025002.